Journal of Alloys and Compounds 540 (2012) 67–74

Contents lists available at SciVerse ScienceDirect

Journal of Alloys and Compounds

journal homepage: www.elsevier.com/locate/jalcom

A study of the luminescence in near UV-pumped red-emitting novel Eu^{3+}-doped $Ba_3Ca_3(PO_4)_4$ phosphors for white light emitting diodes

G.R. Dillip [a], B. Deva Prasad Raju [a,b,*]

[a] Department of Physics, Sri Venkateswara University, Tirupati 517 502, India
[b] Department of Future Studies, Sri Venkateswara University, Tirupati 517 502, India

ARTICLE INFO

Article history:
Received 8 May 2012
Accepted 2 June 2012
Available online 22 June 2012

Keywords:
Inorganic phosphors
Diffuse reflectance spectroscopy
FE-SEM
White LEDs

ABSTRACT

Rare-earth ions doped inorganic luminescent materials (phosphors) in nanodimensions find widespread scientific and industrial applications. This paper report a novel red-emitting Eu^{3+} doped $Ba_3Ca_3(PO_4)_4$ phosphors in nanodimensions were synthesized via one-step conventional solid state reaction method for first time at high temperature in air atmosphere. The morphology and nanostructures of synthesized phosphors were determined by powder X-ray diffraction (XRD), Field emission scanning electron microscopy (FE-SEM) and Energy-dispersive X-ray spectroscopy (EDS). The XRD observation reveals that the undoped and Eu^{3+} doped $Ba_3Ca_3(PO_4)_4$ phosphors are in single crystalline phase with the sizes of 40–65 nm. FE-SEM image indicated the phosphor is composed of nearly spherical particles and rod like structures with several nanometer sizes. The presence of orthophosphates in $Ba_3Ca_3(PO_4)_4$ phosphor was identified by Fourier transform infrared (FT-IR) analysis and the thermal stability was studied by Differential scanning calorimetry (DSC). Diffuse reflectance spectra (DRS) evidenced the incorporated Eu^{3+} ions in host material. In addition, the bandgap of these samples were estimated from the Mubelka–Munk function. The room-temperature photoluminescence spectra show the characteristic red fluorescence originating from intra 4f $^5D_0 \rightarrow {}^7F_2$ (616 nm) transition of Eu^{3+} is observed by introducing Eu^{3+} ions in $Ba_3Ca_3(PO_4)_4$ phosphors. The calculated color coordinates are lies in the orange–red region. Therefore, these obtained results suggest that the prepared phosphors exhibit great potential for use as red-component for near ultraviolet white light emitting diodes (NUV WLEDs).

1. Introduction

Now-a-days, the synthesized particles in nanoscale are essential for ongoing device improvements and miniaturization. The nanoparticles are needed for a better display resolution, smaller pixel sizes and so on. The phosphate-based luminescent materials in nanodimensions have received considerable attention owing to their potential application in solid-state lighting, which could be supplanting the conventional incandescent and fluorescent lamps in the coming future. Rare-earth ions doped nanometer sized powder phosphors have emerged as a new class of luminescence materials with superior performance characteristics such as high stability, brightness and flexible over their micrometer counterparts [1–3]. The technological applications of lanthanide inorganic luminescent materials embraces not only display devices, such as plasma display panel (PDP) and field emission display (FED), but also lasers, optoelectronics and also as fluorescent markers in biomedicine [4–6]. Rare earth ions have been playing an important role in modern lighting and display field due to the abundant emission colors based on their 4f–4f or 5d–4f transitions. Currently, much effort have been directed towards white light emitting diodes (WLEDs) owing to their excellent properties such as long lifetime, high durability, low power consumption, high luminescence efficiency and environmental friendliness [7–10]. Owing to their strong red emission, mainly research is focused on novel Eu^{3+} doped nanocrystalline materials. For instance, many efforts have been paid to investigate the properties of nanodimension $Y_2O_2S:Eu^{3+}$ and $Y_2O_3:Eu^{3+}$ due to its the unprecedented red emitting phosphor with chemical stability under UV or VUV excitation. Unfortunately, the $Y_2O_2S:Eu^{3+}$ and $Y_2O_3:Eu^{3+}$ based phosphors has low emission efficiency and are relatively expensive. From the view point of WLEDs applications, in order to supplant these devices, it is necessary to explore the non-rare-earth hosts with low costs and high quantum efficiency, because in many cases, the quantum efficiency for red emission is still limited [11–14]. To obtain red luminescent materials with high quantum efficiencies, several factors, including the nature of host matrix, energy transfer, and lattice modifications, should be taken into account.

A series of rare-earth ions doped phosphate host phosphors such as $KCaPO_4$ [15], $NaCaPO_4$ [16], $NaBaPO_4$ [17], $SrMg_2(PO_4)_2$

* Corresponding author at: Department of Future Studies, Sri Venkateswara University, Tirupati 517 502, India.
E-mail address: drdevaprasadraju@gmail.com (B. Deva Prasad Raju).

0925-8388/$ - see front matter © 2012 Elsevier B.V. All rights reserved.
http://dx.doi.org/10.1016/j.jallcom.2012.06.009

[18], $BaCaP_4O_{12}$ [19], $Ba_{1.6}Ca_{0.4}P_2O_9$ [20] and others have been reported. Recently, several methods have been employed for the synthesis of polycrystalline phosphors in nanoscale: co-precipitation method [21], combustion method [22], sol–gel method [23] and others. Herein, we applied the single pot conventional solid state reaction method at high temperature to synthesize the Eu^{3+}:$Ba_3Ca_3(PO_4)_4$ nanocrystals. In addition, this synthesis method is an effective and in expensive procedure for preparation of various useful materials. To the best of our knowledge, no results have been reported on the luminescence of $Ba_3Ca_3(PO_4)_4$ doped with trivalent Eu^{3+} ions. All these samples were characterized by XRD, FTIR, FE-SEM with EDS, DSC followed by the spectroscopic studies of excitation and emission and also UV–Vis DRS.

2. Experimental

Polycrystalline samples of Eu^{3+}:$Ba_3Ca_3(PO_4)_4$ were synthesized by a solid-state reaction method at high temperature. All the chemicals are of analytical purity $BaCO_3$, $CaCO_3$, $NH_4H_2PO_4$ and Eu_2O_3 (99.99%) were used as received without further purification. The nominal Eu^{3+} content was varied from 0 to 7 at.% in host material. First, the stiochiometric mixture of the above mentioned raw materials were thoroughly mixed and ground together in an agate mortar for 1 h. Each of the powder mixtures was put into porcelain crucibles, and was placed in an electric furnace, sintered at 1000 °C for 6 h. After sintering, the samples were cooled to room temperature in the furnace, and ground again into powder for further measurements.

The phases of prepared samples were identified by powder X-ray diffraction analysis on a Siemens X-ray diffractometer AXS D 5005 with CuKα radiation (λ = 1.5406 Å) at 40 kV and 20 mA and the 2θ range was varied between 10° and 60°. To elucidate the structure of these phosphors, the Fourier transform infrared spectroscopy (FT-IR) analysis was carried out on a Perkin Elmer spectrophotometer in the range 4000–450 cm^{-1} using KBr pellets. Thermal studies were carried out on a Metler Toledo DSC1 at a heating rate of 10 °C/min under Nitrogen atmosphere. The temperature range was varied from 30 to 450 °C. The morphology of the phosphor was inspected by use of a field emission scanning electron microscope (FE-SEM; SUPRA 55, CARL ZEISS, GETMANY). To identify the presence of constituents in the prepared phosphor, an energy dispersive X-ray spectroscopy was employed equipped with an X-ray detector attached to FE-SEM instrument. UV–Vis diffuse reflectance spectra were recorded on V-670 UV–Vis-NIR spectrophotometer (JASCO, JAPAN). The measurements of the photoluminescence excitation (PLE) and photoluminescence (PL) spectra were performed using a Jobin Vyon Fluorolog – 3 fluorescence spectrophotometer equipped with a Xenon lamp and the decay curve measurements were also recorded on the same instrument. All the measurements were recorded at room temperature.

3. Results and discussion

The XRD patterns of activator, Eu^{3+} (0, 1, 3, 5 and 7 at.%) doped $Ba_3Ca_3(PO_4)_4$ phosphors are shown in Fig. 1. The XRD pattern of $Ba_3Ca_3(PO_4)_4$ crystal (JCPDS Card No: 24-0091) is also shown in figure for comparison. It is clear from the figure that the introduction of an activator Eu^{3+} ion has not caused any significant changes to the crystal structure of $Ba_3Ca_3(PO_4)_4$. Hence, the phosphors prepared by solid state reaction method are single phase orthophosphates without any secondary phases.

It is regarded that the trivalent Eu^{3+} ions occupy the bivalent Ca^{2+}/Ba^{2+} and pentavalent P^{5+} ions in the host lattice, because the radius of Ba^{2+}, Ca^{2+}, P^{5+} and Eu^{3+} for coordination number (CN = 8) are 0.147, 0.112, 0.017 and 0.107 nm, respectively [24–26]. According to the equation [16,27],

$$D_r = 100 \times [R_m(CN) - R_d(CN)]/R_m(CN) \quad (1)$$

the radius percentage difference between doped (Eu^{3+}) ions and the possible substituted ions (Ca^{2+}, Ba^{2+} and P^{5+}) in host are calculated, where D_r is the radius percentage difference, CN the coordination number, R_m(CN) the cation radius of the host, and R_d(CN) the radius of doped ion. The estimated values of D_r between Eu^{3+} and Ca^{2+} and Eu^{3+} and Ba^{2+} on eight-coordinated sites are 4.4% and 27%, respectively, while the value of D_r between Eu^{3+} and P^{5+} is −529.41%. From the survey of literature, it is noticed that the acceptable percentage difference in ionic radii between doped and substituted ions must not exceed 30% [28]. Hence, we believed that there may be two different luminescent centers in $Ba_3Ca_3(PO_4)_4$:Eu^{3+}, which corresponds to Ca^{2+}/Ba^{2+} sites substituted by trivalent Eu^{3+} ions, because of their similar ionic radii. Hence, the authors assumed that the charge loss is most probably compensated by Ca^{2+}/Ba^{2+} vacancies ($V_{Ca/Ba}$), described by

$$3Ca^{2+}/Ba^{2+} \rightarrow 2Eu^{3+} + V_{Ca/Ba} \quad (2)$$

From the XRD data, the average crystallite size of undoped and Eu^{3+} doped $Ba_3Ca_3(PO_4)_4$ particles is determined using Scherrer relation,

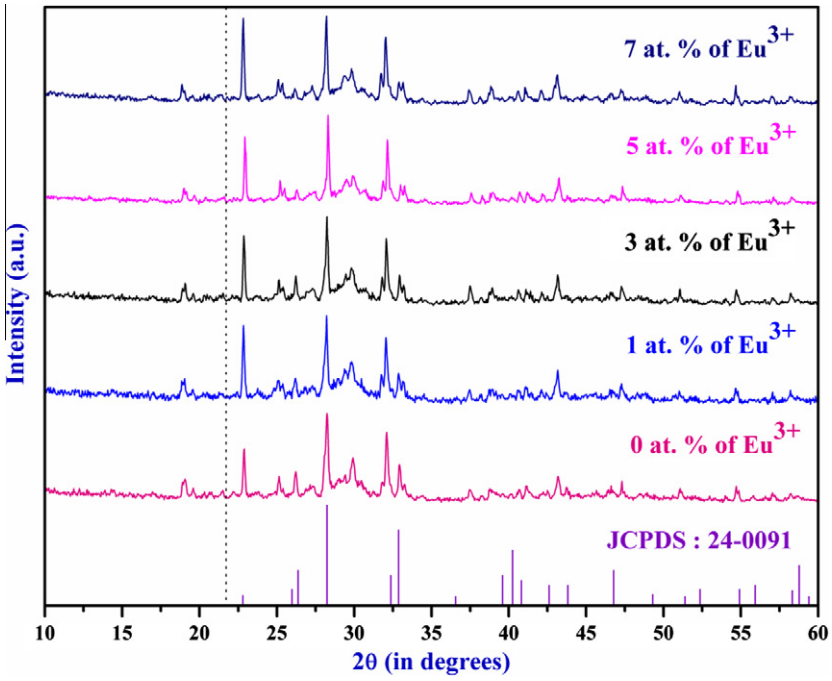

Fig. 1. XRD patterns of Eu^{3+}:$Ba_3Ca_3(PO_4)_4$ phosphors.

Table 1
Variation of Bragg's angle, crystallite size, energy gap, asymmetric ratio and lifetimes with the Eu^{3+} content in $Ba_3Ca_3(PO_4)_4$ phosphors.

S. No.	Nominal Eu^{3+} content in host (at.%)	Peak position of Bragg's angle 2θ (degree)	Crystallite size (nm)	Calculated energy gap (± 0.04 eV)	Asymmetric ratio (E/M)	Lifetimes τ (ms)
1	0	28.24	41.88	5.96	–	–
2	1	28.21	46.35	5.86	1.31	2.03
3	3	28.24	52.06	5.82	1.23	2.07
4	5	28.30	63.11	5.67	1.20	2.18
5	7	28.20	50.58	5.77	1.26	2.14

$$D_{hkl} = k\lambda/[\beta_{2\theta}\cos(\theta)] \quad (3)$$

where $\beta_{2\theta}$ is the full width half maximum (FWHM) at 2θ in radians, k is the constant (0.89), λ is the wavelength of X-rays (0.15406 nm), θ is the diffraction angle and D_{hkl} is the average crystallite size along (h k l) directions. The average crystallite sizes of the phosphors are estimated, which is in the range 40–65 nm and are shown in the Table 1. The variation of Bragg's angle due to the incorporated Eu^{3+} ions in $Ba_3Ca_3(PO_4)_4$ host matrices were depicted in Fig. 2. It is clear from the figure that with increase the doping concentration of Eu^{3+} ions, the intensity of $Ba_3Ca_3(PO_4)_4$:Eu^{3+} phosphors were also increased up to the 5 at.% and further increase of doping concentration, the intensity is decreased due to the concentration quenching effect. This is due to the increase of doping concentration, results the decrease of crystallilty and increase of disorder effect, which resulted in the broadening and decreases of intensity of the XRD peaks. It is observed from the table that the various sizes of the particles are due to the smaller ionic radii of Eu^{3+} compared to that of cations (Ca^{2+}/Ba^{2+}) [29] and the similar results were also observed in DRS and lifetime measurements and the supporting results are also discussed in their appropriate sections.

To identify the presence of orthophosphate in the synthesized sample, the FTIR spectrum is recorded and shown in Fig. 3. Usually, the IR absorption band at $(PO_4)^{3-}$ groups are located at two region of 1120–940 and 650–540 cm^{-1} [30]. The obtained spectrum consists of the couple of strong and sharp peaks are located at 558 and 1019 cm^{-1} and these are assigned to bending and stretching vibrations of orthophosphate $[(PO_4)^{3-}]$ groups. The two weak absorption bands identified at 1415 and 3430 cm^{-1} are clearly indicated the presence of OH group in the samples. These bands are the characteristic vibrations of water from air, physically absorbed on the sample surface [31]. It is known that the presence of OH content increases the optical losses and then decreases the quantum efficiency of rare-earth doped materials. However, for the present phosphors, the intensity of the IR band associated to OH group is extremely low, which indicates that these studied phosphors are suitable for practical applications. It clearly shows that all vibration comes from the anionic groups of (PO_4) units and there is no polyphosphates in the sample, which is found to be, compared quite well the results reported in literature [32].

In order to examine the actual size and to study the surface morphology of the prepared phosphor, FE-SEM measurement was carried out. The low magnification FE-SEM image of $Ba_3Ca_3(PO_4)_4$:Eu^{3+} (5 at.%) phosphor is shown in Fig. 4a. From this image, it can be observed that the particles have irregular morphology. However, the product is composed of spherical particles and rodlike structure morphologies and that some of the adjacent rods are connected by bridges [33]. A typical high magnification FE-SEM image of prepared phosphor is shown in Fig. 4b. On the careful observation, the average sizes of the particles might be in nanometer range, which is in favor of its application in LEDs. Further, the estimated sizes of the particles are comparable with the particle size obtained from Scherrer relation. Hence, it might be suitable for fabricating the solid-state lighting (SSL) devices.

Detailed composition of the prepared $Ba_3Ca_3(PO_4)_4$:Eu^{3+} (5 at.%) phosphors is further analyzed by EDS. A representative EDS spectrum is shown in Fig. 5. EDS spectrum shows several specific line, the signal of Ba, Ca, P, O and Eu elements in the prepared samples. This confirms the phase purity of the obtained phosphor and is in consistent with XRD analysis.

Fig. 6 shows the DSC trace of $Ba_3Ca_3(PO_4)_4$:Eu^{3+} (5 at.%) phosphor. In the temperature range from 30 to 450 °C, the sample shows only a single endothermic peak centered at 390 °C is due to the removal of CO_2 gases that occurs from the starting materials. No other significant peaks are identified in this range, which clearly indicating that the thermodynamically stable $Ba_3Ca_3(PO_4)_4$:Eu^{3+} phosphor was obtained [34].

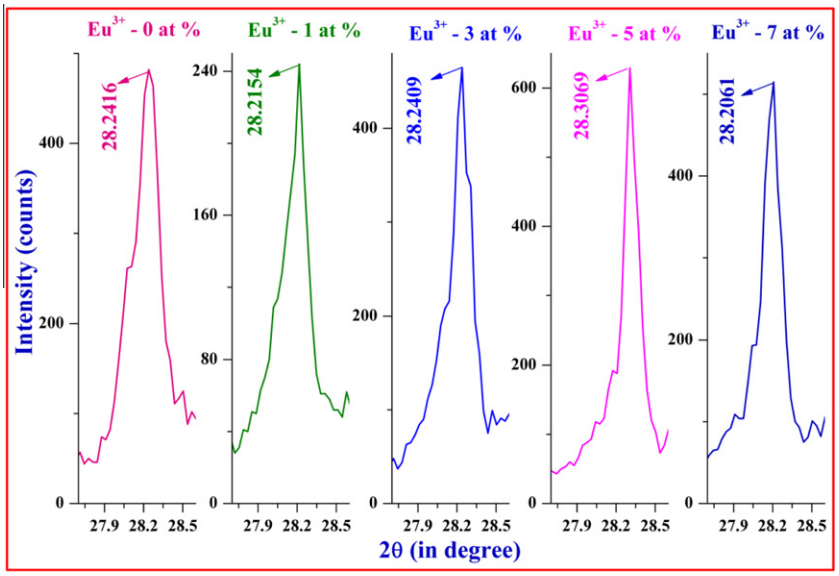

Fig. 2. Variation of Bragg's angle of $Ba_3Ca_3(PO_4)_4$ powder products associated with the different Eu^{3+} ion concentrations.

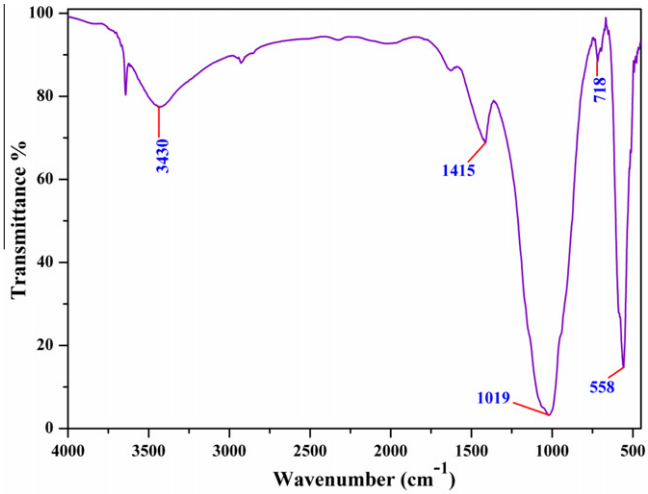

Fig. 3. FTIR spectrum of $Ba_3Ca_3(PO_4)_4:Eu^{3+}$ (5 at.%) phosphor.

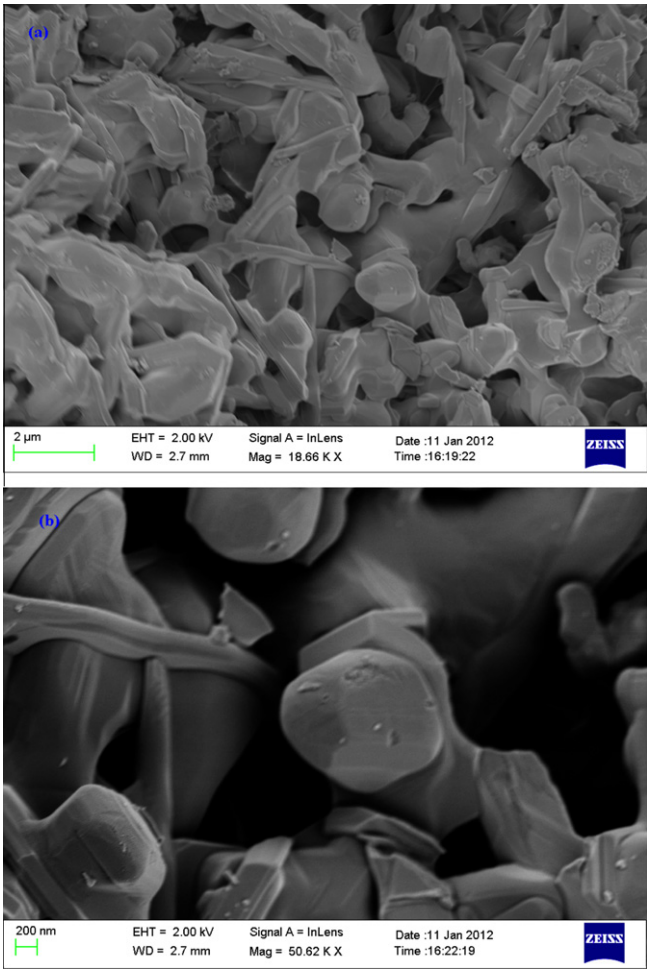

Fig. 4. FE-SEM images of $Ba_3Ca_3(PO_4)_4:Eu^{3+}$ (5 at.%) phosphor: (a) Low-magnification and (b) High-magnification.

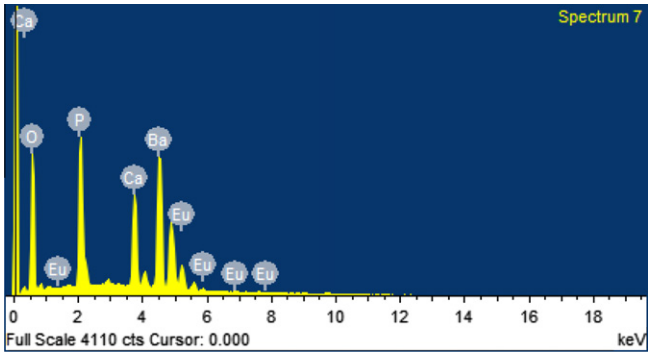

Fig. 5. EDS profile of $Ba_3Ca_3(PO_4)_4:Eu^{3+}$ (5 at.%) phosphor.

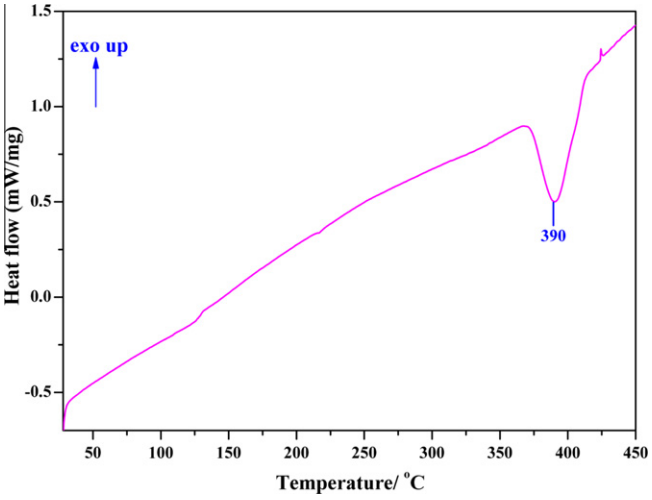

Fig. 6. DSC profile of $Ba_3Ca_3(PO_4)_4:Eu^{3+}$ (5 at.%) phosphor.

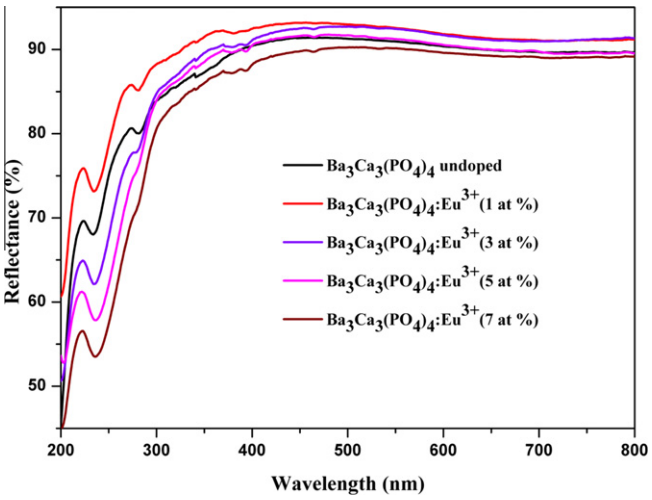

Fig. 7. Diffuse reflectance spectra of $Ba_3Ca_3(PO_4)_4:Eu^{3+}$ phosphors.

Fig. 7 represents the room temperature UV–Vis diffuse reflectance spectra of undoped and Eu^{3+} doped $Ba_3Ca_3(PO_4)_4$ powder samples. As shown in figure, the sharp absorption bands appeared in the range 230–340 nm have similar shapes for all samples, while many sharp absorption peaks in the range 375–550 nm are found in the DRS of the Eu^{3+} doped samples. In the wavelength range 230–340 nm, the sharp absorption bands at 235, 281 and 340 nm are attributed to the charge transfer from the O ligands to the central P atom inside the $(PO_4)^{3-}$ groups. The sharp peaks at 379, 393, 465, 510, 534 and 547 nm are due to the 4f–4f inner shell transitions of Eu^{3+} ions [35–37]. The careful observation reveals that,

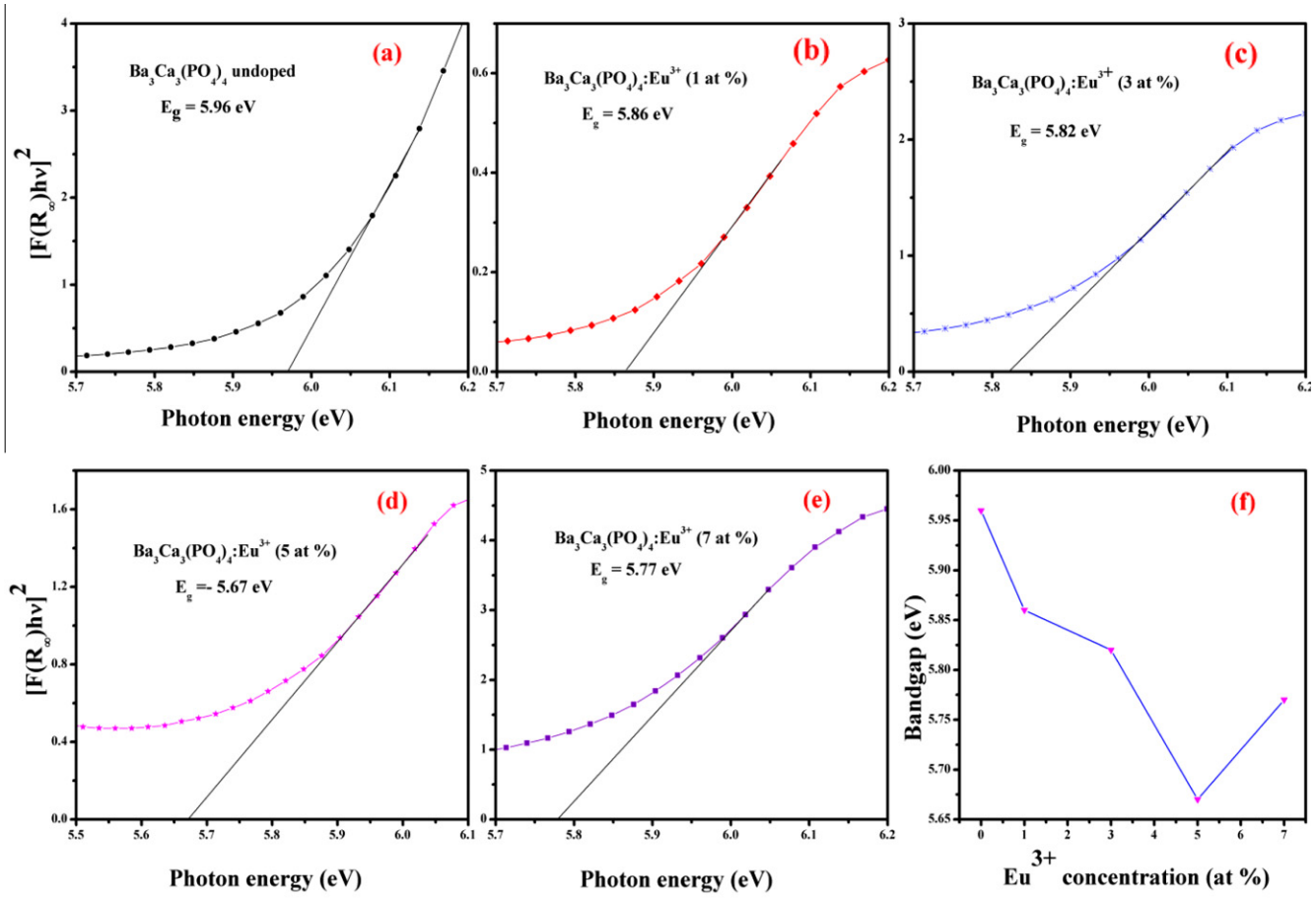

Fig. 8. (a–e) Kubelka–Munk transformed reflectance spectra of $Ba_3Ca_3(PO_4)_4$:Eu^{3+} and (f) The variation of optical bandgap of $Ba_3Ca_3(PO_4)_4$ associated with Eu^{3+} concentration.

with the increasing of the dopant Eu^{3+} concentration, the absorption bands also gradually increased, indicating the incorporation of dopant ions into the host lattices.

The bandgap of the powder samples were determined by a more convenient diffuse reflectance spectroscopy technique in the UV–Vis spectral range. Generally, the Kubelka–Munk equation is used to convert the reflectance into equivalent absorption spectra. Therefore, the DRS were analyzed by the Kubelka–Munk absorption co-efficient (K/S), using the following relation [38,39],

$$K/S = (1 - R_\infty)^2/2R_\infty = F(R_\infty)\alpha\alpha = (h\nu - E_g)^{1/2}/h\nu \quad (4)$$

where K and S are the absorption and scattering coefficients, respectively and R_∞ denotes the diffuse reflectance of an infinitely thick sample, $F(R_\infty)$ is the K–M function, $h\nu$ is the photon energy and E_g is the bandgap energy for direct transition. The bandgap energies of undoped and Eu^{3+} doped samples were estimated from the variation of the Kubelka–Munk function $[F(R)h\nu]^2$ with photon energy ($h\nu$), which is represented in Fig. 8a–e. The estimated bandgap energies are in the range from 5.67 ± 0.04 to 5.96 ± 0.04 eV, listed in Table 1. Fig. 8f shows the variation of bandgap with the incorporated Eu^{3+} ions into $Ba_3Ca_3(PO_4)_4$ host. The increase of dopant concentration accompanies enhancement of the absorption, and also a gradual shifting towards the higher wavelengths region of the absorption edge [40]. It is clear from the figure that with the increasing of incorporated Eu^{3+} content, the bandgap energy of the $Ba_3Ca_3(PO_4)_4$ powders decreased up to 5 at.% of Eu^{3+} and slightly increased for 7 at.% of Eu^{3+}, which is agreement well with those results obtained from XRD results. Hence, we observed a red shift in the bandgap of Eu^{3+} doped phosphors with the increase of doping concentration, similar results were reported earlier in literature. For instance, Yu et al. [41] observed an enhancement of absorption in the visible range and red shift (i.e. lower energy) of the bandgap on Fe^{3+} doped TiO_2 nanotubes. This behavior has been explained by quantum confinement effect i.e. the $Ba_3Ca_3(PO_4)_4$ creates the dopant levels near the valence band with the incorporation of Eu^{3+} ions and it provides an efficient absorption pathways for visible light. From the survey of literature, it is noticed that the relative shift of the absorption edge of materials depends on the difference between the ionic radius of the dopant and host cations, as well as on the chemical nature of dopant [40].

Fig. 9 shows the excitation spectrum associated with Eu^{3+} (5 at.%) ions doped in $Ba_3Ca_3(PO_4)_4$ monitored at 616 nm at room temperature. In the wavelength range 350–550 nm, the spectrum contains several sharp lines due to the intra 4f–4f transition of Eu^{3+} in the host lattice, similar sharp lines are also obtained from the diffuse reflectance spectra (Fig. 6). The sharp intense peaks at 362 nm ($^7F_0 \rightarrow {}^5D_4$), 382 nm ($^7F_0 \rightarrow {}^5L_7$), 394 nm ($^7F_0 \rightarrow {}^5L_6$), 415 nm ($^7F_0 \rightarrow {}^5D_3$), 465 nm ($^7F_0 \rightarrow {}^5D_2$) and 526/533 nm ($^7F_0 \rightarrow {}^5D_1$) are the characteristic transitions of Eu^{3+} ions in host lattice [42]. Among, these several sharp lines, the dominant intense excitation peak lies at 394 nm corresponding to $^7F_0 \rightarrow {}^5L_6$ transition is used to study the emission spectra for all samples.

In order to further investigate the effect of doped Eu^{3+} concentration on the luminescence intensity of $Ba_3Ca_3(PO_4)_4$ phosphors, the photoluminescence emission studies have been carried out. Fig. 10 presents the emission spectra of $Ba_3Ca_3(PO_4)_4$ phosphors for various Eu^{3+} concentrations. The emission spectra recorded

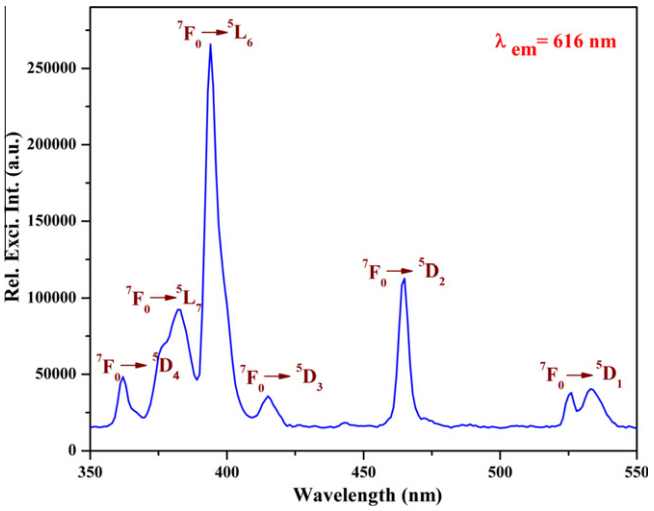

Fig. 9. Excitation spectrum of $Ba_3Ca_3(PO_4)_4:Eu^{3+}$ (5 at.%) phosphor.

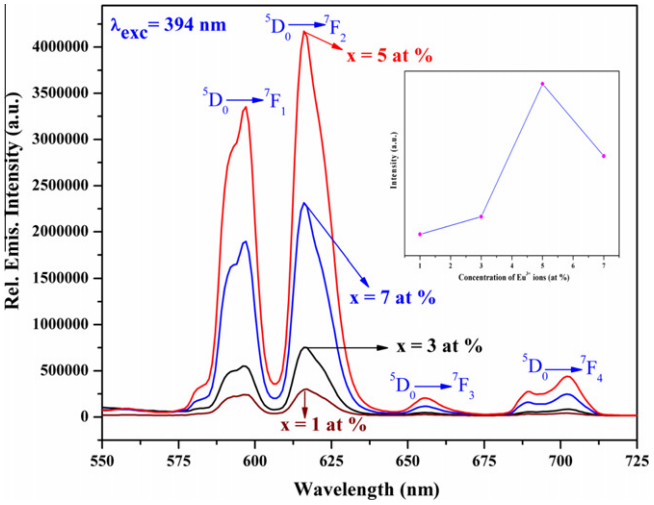

Fig. 10. Emission spectra of $Ba_3Ca_3(PO_4)_4:Eu^{3+}$ phosphor. The inset shows variation of PL intensity with Eu^{3+} content.

upon excitation wavelength $\lambda = 394$ nm consist of typical sharp lines ranging from 550 to 725 nm, corresponding to transition from the excited $^5D_0$ level to ^7F_J ($J = 1, 2, 3$ and 4) levels of Eu^{3+} activators [43]. Since, no transitions related to $^5D_0 \rightarrow {}^7F_5$ and $^5D_0 \rightarrow {}^7F_6$ were experimentally detected. It is seen that, for all samples, the emission spectra are similar in shape, and the peaks differ in their relatively intensities. Among the several sharp peaks, we noticed that the most intense red emission at 616 nm for all samples. The energy level diagram of Eu^{3+} ions in $Ba_3Ca_3(PO_4)_4$ phosphor is depicted in Fig. 11. Generally, the orange emission at 597 nm from $^5D_0 \rightarrow {}^7F_1$ transition is of pure magnetic dipole character and therefore independent from the local symmetry of Eu^{3+} ions, while the red emission at 616 nm from $^5D_0 \rightarrow {}^7F_2$ transition is of pure electric dipole character and hence dependent on the ligand-field surrounding of the Eu^{3+} ions. However, the magnetic dipole transition ($^5D_0 \rightarrow {}^7F_1$) probability does not change even in low symmetry systems, because they are parity – allowed, which allows use of the intensity of this transition as an internal reference. An electric dipole transition ($^5D_0 \rightarrow {}^7F_2$) with $\Delta J = 2$ is hypersensitive to the crystal field environment. For instance, in a site with inversion symmetry, the magnetic dipole transition is dominant, while in low symmetry systems, the electric dipole transition

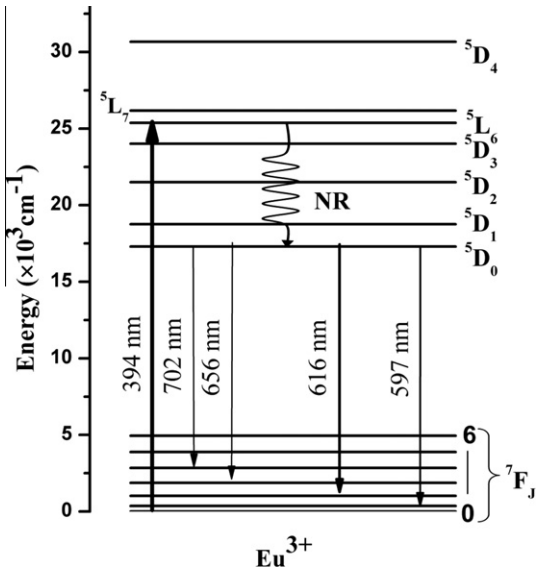

Fig. 11. The schematic energy level diagram of Eu^{3+} ions in $Ba_3Ca_3(PO_4)_4$ phosphor.

($^5D_0 \rightarrow {}^7F_2$) dominates the emission spectrum [1,44,45]. Therefore, the relative integrated intensity ratio of the transitions $^5D_0 \rightarrow {}^7F_2$ to $^5D_0 \rightarrow {}^7F_1$ (the so-called asymmetric ratio) is very sensitive to the local environment. The asymmetric ratio [3],

$$E/M = I(^5D_0 \rightarrow {}^7F_2)/I(^5D_0 \rightarrow {}^7F_1) \quad (5)$$

It can be also used as a good indicator to examine any change of the symmetry of Eu^{3+} sites. From the spectra, it is observed that the intensity of the electric dipole transition is much higher than that of the magnetic dipole transition. The calculated asymmetric ratios of all samples are presented in Table 1. The E/M ratio varies from 1.20 to 1.31. It is evident that the Eu^{3+} ion has no inversion symmetry. It is noticed that the local symmetry is not significantly affected by the Eu^{3+} dopant content in the host and there was no much influence on the morphology and size of the particle. This is in agreement with the increasing particle size as calculated from the Scherrer's formula. Well known to all, the lower concentrations of dopant lead to weak luminescence, while the high concentrations of activator cause concentration quenching. With the increase of Eu^{3+} content, the dominant red emission gradually increases reached maximum for 5 at.% and further increase of dopant concentration, the intensity decreased for 7 at.%. The concentration quenching effect is due to the rise in the number of non-radiative decay channels, as promoted by the interaction with quenching centers during the cross relaxation or energy transfer process between excited and unexcited Eu^{3+} ions. Therefore, the solubility of Eu^{3+} content in host was found to be 5 at.%.

In order to obtain additional information on the luminescence properties of Eu^{3+} ions in $Ba_3Ca_3(PO_4)_4$ phosphors, the decay curves have been measured. Fig. 12 shows the decay curves for $^5D_0 \rightarrow {}^7F_2$ (616 nm) emission for these samples when excited at 394 nm. All the decay curves are well fitted by the single-exponential equation [46],

$$I = I_0 \exp(-t/\tau) \quad (6)$$

where I and I_0 are the luminescence intensity at time t and 0, respectively, and τ is the PL lifetime. The estimated lifetime values from the fits are presented in Table 1. The single exponential behavior of fits for all samples evidences the presence of the Eu^{3+} environment is unique in according to the crystal structure. In addition, there is no wavelength shift or peak for new site has been observed for various concentrations. This strongly suggests that the local

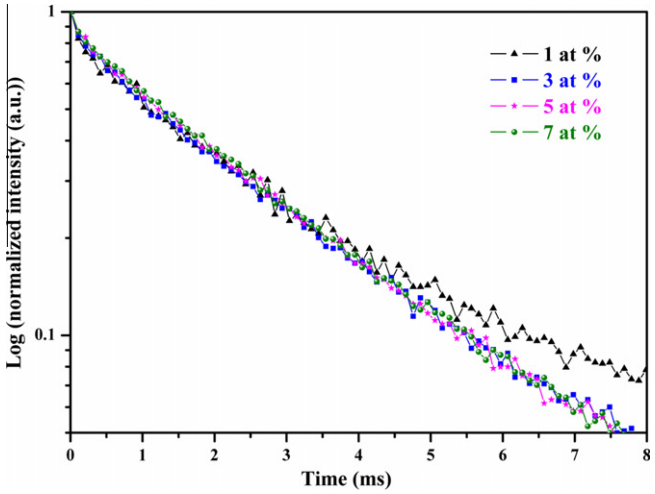

Fig. 12. Photoluminescence decay curves of $Ba_3Ca_3(PO_4)_4:Eu^{3+}$ phosphors (excited at 394 nm, monitored at 616 nm).

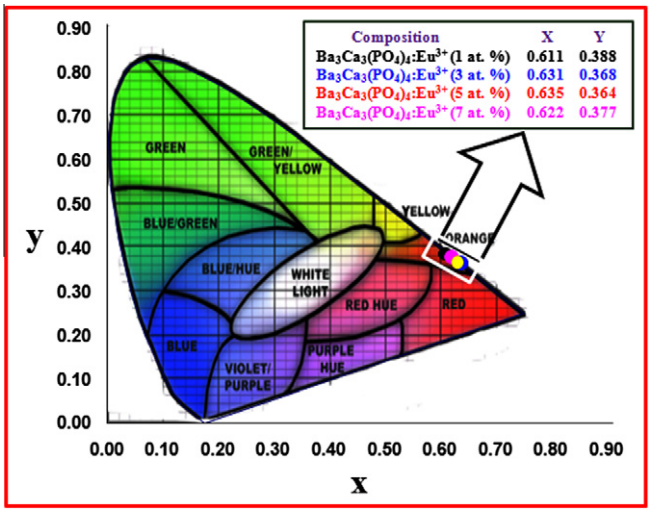

Fig. 13. CIE chromaticity diagram for $Ba_3Ca_3(PO_4)_4:Eu^{3+}$ phosphors.

environment of the Eu^{3+} ions in the lattice is the same in different positions. It is noticed from the table that the slight variation of lifetime values for different concentrations may be due to the different particle sizes of the synthesized phosphors, which is in consistent with those results obtained from XRD analysis.

In general, the emission color of two phosphors is compared by means of color coordinates and is a good certification for photoluminescence applications. In 1931, the Commission International de l'Eclairage (CIE) established a universal quantitative model of color space. The chromaticity coordinates of Eu^{3+} doped $Ba_3Ca_3(PO_4)_4$ phosphors are calculated (using CIE calculate software) from their corresponding emission spectra excited by 394 nm and have shown in Fig. 13. The obtained color coordinates of these samples are lies in the orange-red region. The changes in the color coordinates may be due to the variation of the asymmetric ratios of various concentrations of Eu^{3+} ion in $Ba_3Ca_3(PO_4)_4$ phosphors. Further, the present color coordinates are comparable with the commercially available red phosphor of $Y_2O_2S:Eu^{3+}$ (0.622, 0.351) [47].

4. Conclusions

In summary, a series of novel $Ba_3Ca_3(PO_4)_4:Eu^{3+}$ red-emitting phosphors were synthesized via the high temperature solid-state reaction method. XRD and FTIR analysis indicate that these phosphors exhibit a single phase orthophosphates without any polyphosphates and the sizes of particles are found to be 40–65 nm range. It is evident from the FE-SEM analysis that the phosphor is formed by nearly spherical and to even rodlike crystallite, which is in several nanometers. UV–Vis diffuse reflectance spectra of these phosphors exhibited a little red shift (i.e. lower energy) due to the Eu^{3+} content in host matrices. Moreover, the optical bandgap also calculated from the Mubelka–Munk function, ranging from 5.67 to 5.96 eV. Photoluminescence spectra of all samples show the characteristic sharp lines of the intra 4f–4f transitions of Eu^{3+} with similar shapes, but changes in their emission intensities. These emission lines were ascribed to $^5D_0 \rightarrow {}^7F_{0-4}$ transitions. The calculated asymmetric ratios indicating the Eu^{3+} ion has no inversion symmetry. Moreover, the optimum Eu^{3+} concentration in $Ba_3Ca_3(PO_4)_4$ host matrix is found to be 5 at.%. The results obtained above demonstrated the potentiality of $Ba_3Ca_3(PO_4)_4:Eu^{3+}$ phosphors as red-component for white LEDs in solid-state lighting application.

Acknowledgements

The authors are sincerely thankful to Spectroscopy/Analytical Test Facility (SATF), Indian Institute of Science, Bangalore and Sophisticated Analytical Instrumentation Facility (SAIF), Indian Institute of Technology, Chennai for extending the instrumental facilities.

References

[1] C. Lorbeer, J. Cybinska, A.V. Mudring, Cryst. Growth Des. 11 (2011) 1040–1048.
[2] M. Yu, J. Lin, J. Fang, Chem. Mater. 17 (2005) 1783–1791.
[3] J.C. Boyer, F. Vetrone, J.A. Capobianco, A. Speghini, M. Bettinelli, J. Phys. Chem. B 108 (2004) 20137–20143.
[4] I. Hemmila, J. Alloys Compd. 225 (1995) 480–485.
[5] Martinus H.V. Werts, Ronald T.F. Jukes, Jan W. Verhoeven, Phys. Chem. Chem. Phys 4 (2002) 1542–1548.
[6] T. Justel, H. Nikol, C. Ronda, Angew. Chem. Int. Ed. 37 (1998) 3084–3103.
[7] T. Kishida, T. Ban, N. Kobayashi, Appl. Phys. Lett. 82 (2003) 3817–3819.
[8] D.K. Yim, I.S. Cho, C.W. Lee, J.H. Noh, H.S. Roh, K.S. Hond, Opt. Mater. 33 (2011) 1036–1040.
[9] Wei-Ren Liu, Chien-Hao Huang, Chih-Pin Wu, Yi-Chen Chiu, Yao-Tsung Yeh, Teng-Ming Chen, J. Mater. Chem. 21 (2011) 6869–6874.
[10] T. Murata, T. Tanoue, M. Iwasaki, K. Morinaga, T. Hase, J. Lumin. 114 (2005) 207–212.
[11] J. Thirumalai, R. Jagannathan, D.C. Trivedi, J. Lumin. 126 (2007) 353–358.
[12] Q. Li, L. Gao, D.S. Yan, Chem. Mater. 11 (1999) 533–535.
[13] S. Yu, Z. Lin, L. Zhang, G. Wang, Cryst. Growth Des. 7 (2007) 2397–2399.
[14] Y. Su, L. Li, G. Li, Chem. Mater. 20 (2008) 6060–6067.
[15] L. Guan, C. Liu, X. Li, G. Jia, Q. Guo, Z. Yang, G. Fu, Mater. Res. Bull. 46 (2011) 1496–1499.
[16] B.K. Grandhe, V.R. Bandi, K. Jang, S.S. Kim, D.S. Shin, Y.I. Lee, J.M. Lim, T. Sond, J. Alloys Compd. 509 (2011) 7937–7942.
[17] X. Li, L. Guan, X. Li, J. Wen, Z. Yang, Powder Technol. 200 (2010) 12–15.
[18] X. Wang, F. Du, D. Wei, Y. Huang, H.J. Seo, Sen. Act. B 158 (2011) 171–175.
[19] H.A. Hoppe, J.M.U. Panzer, Eur. J. Inorg. Chem. 2009 (2009) 3127–3130.
[20] X.M. Zhang, W.C. Li, K.H. Jang, H.J. Seo, Curr. Appl. Phys. 12 (2012) 299–302.
[21] H. Lai, A. Bao, Y. Yang, W. Xu, Y. Tao, H. Yang, J. Lumin. 128 (2008) 521–524.
[22] I.M. Nagpure, V.B. Pawade, S.J. Dhoble, Luminescence 25 (2010) 9–13.
[23] B. Yan, H. Huang, Y. Sui, J. Sol–Gel Sci. Technol. 36 (2005) 95–102.
[24] Pan-Lai LI, Zhi-Jun WANG, Zhi-Ping YANG, Qing-Lin GUO, Chin. Phys. Lett. 28 (2011) 017801–017803.
[25] S. Yan, J. Zhang, X. Zhang, S. Lu, X. Ren, Z. Nie, X. Wang, J. Phys. Chem. C 111 (2007) 13256–13260.
[26] W. Li, M. Wang, Z.H. Li, X.F. Shang, H. Wang, Y.W. Wang, Y.B. Xu, Russ. J. Electrochem. 43 (2007) 1279–1283.
[27] F.B. Cao, L.S. Li, Y.W. Tian, Y.J. Chen, X.R. Wu, Thin Solid Films 519 (2011) 7971–7976.
[28] A.M. Pires, M.R. Davolos, Chem. Mater. 13 (2001) 21–27.
[29] E. Song, W. Zhao, G. Zhou, X. Dou, C. Yi, M. Zhou, J. Rare Earths 29 (2011) 440–443.
[30] Y. Huang, X. Wang, H.S. Lee, E. Cho, K. Jang, Y. Tao, J. Phys. D:Appl. Phys. 40 (2007) 7821–7825.
[31] F. Lei, B. Yan, Solid State Chem. 181 (2008) 855–862.
[32] S. Hachani, B. Moine, A. El-akrmi, M. Ferid, Opt. Mater. 31 (2009) 678–684.
[33] L. Xu, Y. Su, Q. Zhou, S. Li, Y. Chen, Y. Feng, Cryst. Growth Des. 7 (2007) 810–814.

[34] B. Wang, L. Sun, H. Ju, J. Sol–Gel Sci. Technol. 53 (2010) 454–458.
[35] G. Liu, X. Duan, H. Li, H. Dong, Mater. Chem. Phys. 115 (2009) 165–171.
[36] S. Georgescu, E. Cotoi, A.M. Voiculescu, O. Toma, C. Matei, Rom. J. Phys. 55 (2010) 750–757.
[37] H. Yang, J. Shi, M. Gong, H. Liang, J. Rare Earths 28 (2010) 519–522.
[38] P. Kubelka, F.Z. Munk, Z. Tech. Phys. (Leipzig) 12 (1931) 593–601.
[39] W.B. Im, N.N. Fellows, S.P. DenBaars, R. Seshadri, Y.I. Kim, Chem. Mater. 21 (2009) 2957–2966.
[40] M. Pal, U. Pal, J.M. Gracia, Y. Jimenez, F.P. Rodriguez, Nanoscale Res. Lett. 7 (2012) 1–12.
[41] J. Yu, Q. Xiang, M. Zhou, Appl. Catal. B: Environ. 90 (2009) 595–602.
[42] S. Sailaja, S.J. Dhoble, N. Brahme, B.S. Reddy, J. Mater. Sci. 46 (2011) 7793–7798.
[43] G. Ping, X. Wang, Y. Wu, L. Qin, K. Shu, Opt. Mater. 34 (2012) 748–752.
[44] Y.C. Li, Y.H. Chang, Y.F. Lin, Y.S. Chang, Y.J. Lin, J. Alloys Compd. 439 (2007) 367–375.
[45] L.D. Carlos, R.A.S. Ferreira, V. de Zea Bermudez, S.J.L. Ribeiro, Adv. Mater. 21 (2009) 509–534.
[46] A.K. Parchur, R.S. Ningthoujam, S.B. Rai, G.S. Okram, R.A. Singh, M. Tyagi, S.C. Gadkari, R. Tewari, R.K. Vasta, Dalton Trans. 40 (2011) 7595–7601.
[47] D. Wei, Y. Huang, L. Shi, X. Qiao, H. Seo, J. Electrochem. Soc. 156 (2009) H885–H889.